Contents lists available at ScienceDirect

Applied Catalysis B: Environmental

journal homepage: www.elsevier.com/locate/apcatb

Size dependence of uniformed carbon spheres in promoting graphitic carbon nitride toward enhanced photocatalysis

Shizhen Liu[a], Jun Ke[a], Hongqi Sun[b,*], Jian Liu[a], Moses O. Tade[a], Shaobin Wang[a,*]

[a] Department of Chemical Engineering and CRC for Contamination Assessment and Remediation of the Environment (CRC CARE), Curtin University, GPO Box U1987, WA 6845, Australia
[b] School of Engineering, Edith Cowan University, 270 Joondalup Drive, Joondalup, WA 6027, Australia

ABSTRACT

Recently, graphitic carbon nitride (GCN) has been extensively employed as a metal-free, visible-light-responsive photocatalyst. The strong recombination rate of photo-induced charges and small surface area limit its wide applications. In this study, monodisperse carbon nanospheres (CS) with a uniform size were synthesized from resorcinol-formaldehyde resin using different surfactants and then loaded onto GCN via a hydrothermal treatment. It was found that the size of CS influenced the properties and photocatalytic performances of the CS/GCN hybrids. All the CS/GCN catalysts exhibited higher photocatalytic activities in degradation of water contaminants, antibiotic sulfachloropyridazine and methylene blue, under visible light irradiations. Photoluminescence spectra and photocurrent analysis indicated that hybridization with the carbon spheres at 200–500 nm will significantly reduce the electrocarrier recombination of carbon nitride while increase the photocurrent intensity, resulting in much better photocatalysis.

© 2016 Elsevier B.V. All rights reserved.

1. Introduction

In the past two decades, nanocarbons such as carbon nanotubes (CNTs), graphene oxide (GO), reduced graphene oxide (rGO), graphitic carbon nitride (g-C$_3$N$_4$), and other graphene-like materials have attracted worldwide attention as metal-free nanomaterials, due to their large theoretical surface area, high thermal conductivity, unique electronic property, and sp^2-hybridized carbon configuration [1–3]. Studies on metal-free catalysis have demonstrated that nanocarbons can play promising roles in various catalytic processes for energy and environmental applications [4–6].

Recent researches have indicated a bright horizon of solar energy applications by a polymeric semiconductor, graphitic carbon nitride (GCN). The material is composed of polymeric tri-s-triazine building blocks as a layer-stacked, metal-free visible light sensitive photocatalyst [7]. Up to date, GCN is widely tested in water splitting [8], environmental remediation [9], and electronic devices [10–12] because of its unique properties, such as highly chemical/thermal stability and premium electronic properties [13]. It has a tuneable band-gap energy from 2.6 to 3.5 eV which covers the

visible light (up to 477 nm) to ultraviolet spectrum [14,15]. But pristine GCN presents a low electrical conduction and rapid photo-electron depletion, exhibiting an inefficient photon harvesting and a low photocatalytic activity [16–18]. Therefore, hybridized GCN photocatalyts have been extensively explored [19].
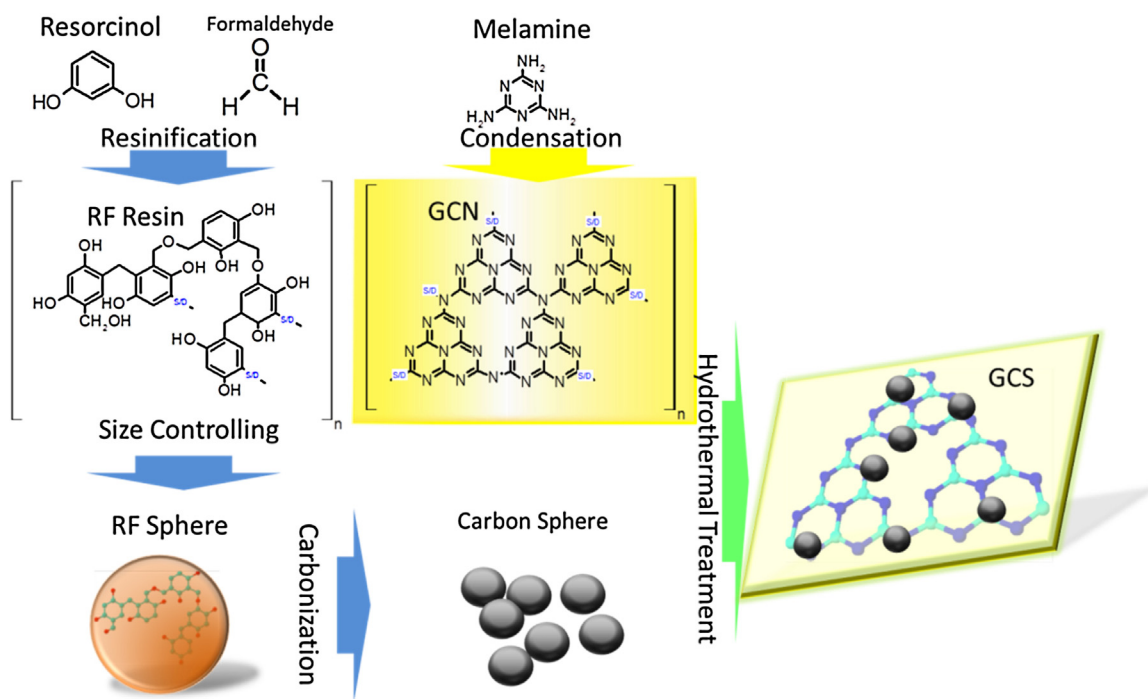
Carbonaceous materials such as graphene oxide (GO) [20], carbon nanotubes (CNTs) [21], and fullerene [22] can accelerate the migration of photo-generated carriers, and then increase the generation of active species in the redox reaction [23,24]. With polar functional groups or long chain molecules, grafting carbonaceous materials over GCN could enlarge the surface area of the catalyst, transform the electron distribution of the particle surface, enhance carrier mobility and weaken the recombination rate of photo-induced electron/hole pairs [25–29].

It was reported that another class of carbonaceous material, resorcinol-formaldehyde carbon spheres (RFCSs), can also exhibit strong environmental compatibility and electric capacity with a low impedance for electron drafting [30–32]. In addition, the dimension of RFCSs could be controlled by either the synthesis or different surfactants [33]. Glucose-based amorphous carbon was successfully loaded on GCN by a hydrothermal method, showing enhanced photocatalysis [34,35]. However, the dimension of carbon sphere was not tailored leaving no control of the surface, electronic and optical properties.

Herein, we present an investigation on the synthesis of RFCS-GCN heterojunction materials for enhanced

Scheme 1. Schematic illustration of the synthesis processes of the GCS samples.

photocatalysis. Controlled uniform size RFCSs were successfully synthesized through varying surfactants and then impregnated on GCN. The effects of CS on the electronic and optical properties as well as photochemical performances (including photodegradation of antibiotics and photocurrent generation) of the GCN materials were evaluated and discussed.

2. Experimental

2.1. Materials

All chemicals used are in analytical grade. Melamine powder (99.9%), resorcinol (≥99.0%), formaldehyde (37 wt.% in H_2O), cysteine (≥99.0%), hexadecyltrimethyl ammonium bromide (CTAB), *tert*-butyl alcohol (≥99.5%), *p*-benzoquinone (≥98%) were provided by Sigma-Aldrich. Pluronic F-127 surfactant, ammonia (25% in water), and ethanol (≥99.9%) were purchased from BASF.

2.2. Preparation of graphitic carbon nitride

Graphitic carbon nitride was prepared through the condensation of melamine. Typically, 10 g of melamine was placed in a 20 mL alumina crucible and well mixed with 10 mL of methanol. The crucible was then moved into an oven to remove methanol at 60 °C for 24 h. After that, the white powder was placed in a muffle furnace for thermal condensation, which was firstly heated to 400 °C at a heating rate of 5 °C/min and kept at this temperature for 2 h, followed by heating to 520 °C with a heating rate of 10 °C/min and keeping for another 2 h. Finally, the yellow product was well ground and labelled as GCN.

2.3. Preparation of resorcinol-formaldehyde carbon spheres

The preparation of uniform resorcinol-formaldehyde (RF) spheres at different sizes follows a similar procedure with varying precursor solutions [33,35]. For 500 nm spheres, 16 mL of pure ethanol and 40 mL of deionized water were mixed in an 80 mL Pyrex bottle in a water bath at 30 °C. Then, 0.2 mL of 25% ammonia

solution was added into the above solution with stirring for 2 h. Later, 0.4 g of resorcinol powder was added in with continuously stirring, until the color of the solution changed to pale brown. After that 0.48 mL of formaldehyde solution was gradually added into the solution and sealed well for 24 h. The dark brown suspension of RF resins was transferred into an 80 mL Teflon-lined autoclave and treated at 100 °C for 24 h. The dark brown RF resin spheres were collected by centrifugation and purified using deionized water for three times and dried at 100 °C in air. The product was referred as 500 RF.

For the preparation of 60 nm RF spheres, a surfactant Pluronic F-127 solution (1.476 mmol/L, water/ethanol) was added into the water/ethanol/ammonia solution before 0.4 g of resorcinol powder was added. The rest of procedure is the same.

For the preparation of 200 nm RF spheres, three surfactants (0.2 g F127, 0.26 g CTAB and 0.4 g cysteine) were mixed with the water/ethanol/ammonia solution before the resorcinol powder was added.

For the preparation of 1000 nm RF spheres, 0.4 mL of 25% ammonia solution was used instead of 0.2 mL to prepare the water/ethanol/ammonia solution.

In the carbonization procedure, RF spheres were put in a furnace tube and heated to 350 °C at a heating rate of 1 °C/min and kept the temperature for 2 h in nitrogen environment, followed by raising the temperature to 600 °C at the same heating rate, maintaining for further 4 h.

2.4. Preparation for GCS hybrid photocatalysts

The CS-GCN photocatalysts were prepared using the prepared carbon spheres and GCN as the precursors by a hydrothermal treatment (Scheme 1). Typically, 1 wt% carbon spheres were mixed with 1 g of the pure GCN in 50 mL of deionization water. After 3 h ultrasonic treatment, the mixed solution was stirred for 3 h at room temperature to generate a homogenous suspension. Then the suspension was moved into a 100 mL Teflon-lined autoclave for a hydrothermal treatment at 150 °C for 12 h. The product was dried at 60 °C. According to the diameter of carbon sphere, the four obtained

samples were referred to GCS-60, GCS-200, GCS-500 and GCS-1000, respectively.

2.5. Characterizations

The crystalline structure of the as-prepared samples were analyzed using powder X-ray diffraction (XRD) technology on a D8-advance X-ray diffractometer using a Cu Kα with 40 kV voltage and 40 mA current. Fourier transform infrared spectroscopy (FTIR) was performed on a Perkin-Elmer FTIR-100 with a MIR detector. UV–vis diffuse reflectance spectra (UV–vis DRS) of the samples were recorded on a JASCO V670 spectrophotometer with an Ø60 mm integrating sphere and $BaSO_4$ as a reference material. Field emission scanning electron microscopy (FE-SEM) was carried out on Zeiss Neon 40EsB was used to determine the morphology, size and surface feature of the samples. Raman spectroscopy was processed on RFS100 Raman with 1064 nm laser source at 400 μW. The Brunauer-Emmett-Teller (BET) surface area and pore size distribution were evaluated using a Quantachrome Autosorb AS-1. The Mott–Schottky plots and photocurrent tests were conducted on a Zennium electrochemical workstation in a conventional three-electrode cell, in which Hg/Hg_2Cl_2 was applied as the reference
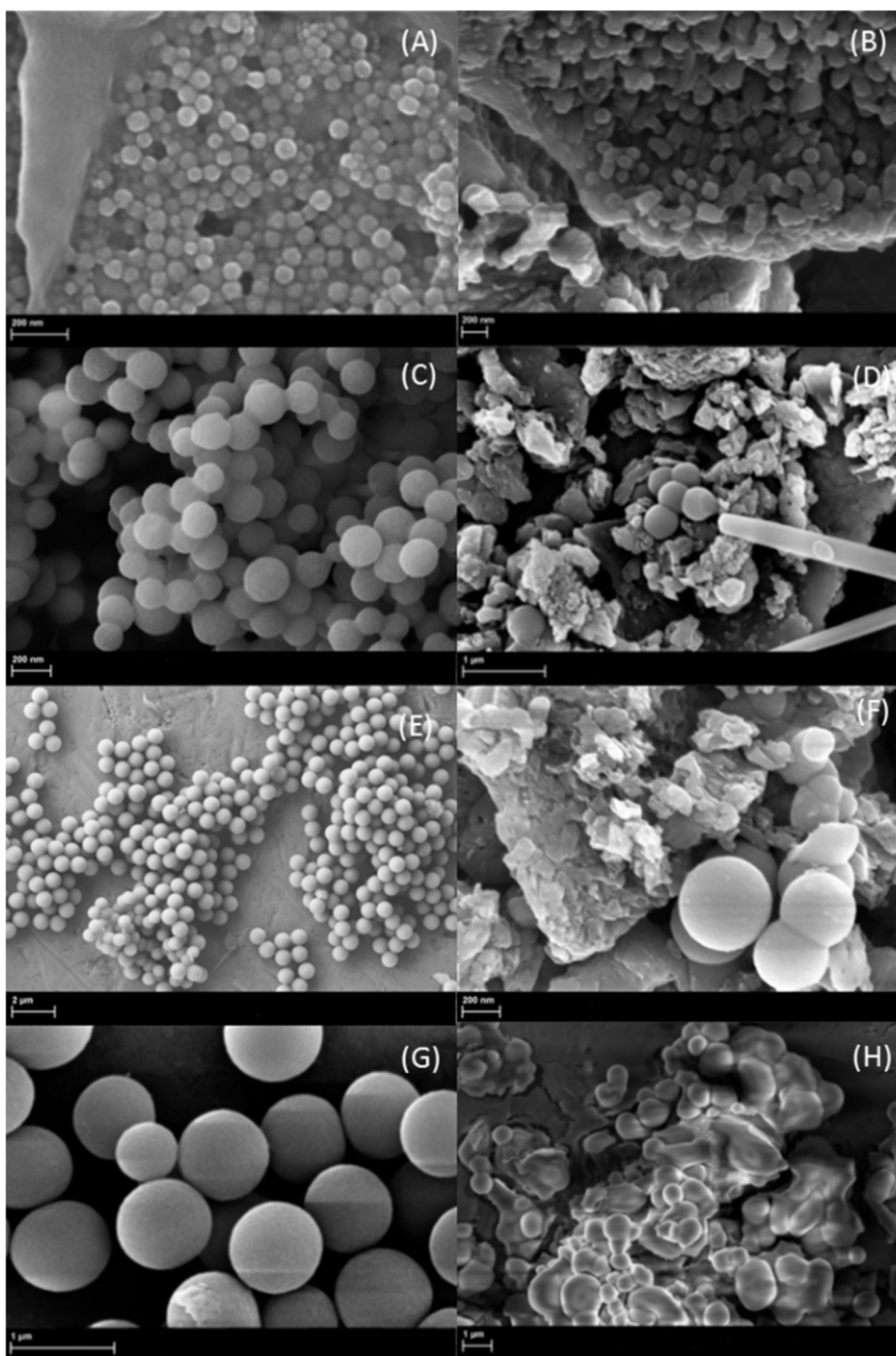

Fig. 1. SEM images of RF spheres at 60 nm (A), 200 nm (C), 500 nm (E) and 1000 nm (G) and GCS-60 (B), GCS-200 (D), GCS-500 (F) and GCS-1000 (H).
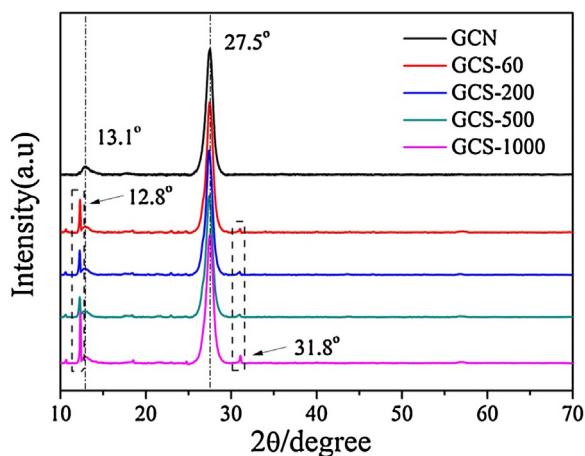
Fig. 2. XRD patterns of GCN, GCS-60, GCS-200, GCS-500 and GCS-1000.

Fig. 3. Raman spectra of GCN, GCS-60, GCS-200, GCS-500 and GCS-1000.

electrode, a platinum wire as the auxiliary electrode, and Na_2SO_4 solution (0.2 M) as an electrolyte. Five cycles were applied and the intermission for turning on/off light was 30 s.

2.6. Photocatalytic activity testing

Photocatalytic performances of CS-GCN photocatalysts were evaluated by degradation of an antibiotic, sulfachloropyridazine (SCP, 30 mg/L), and methylene blue (MB, 10 mg/L) in water solution under artificial sunlight irradiations. In a typical procedure, 200 mL of SCP or MB solution and 100 mg photocatalyst were put into a 1 L glass double-jacket cylindrical reactor with water cycling at 25 °C. The reaction vessel was positioned 30 cm away from the light source, a metal halide lamp with the intensities at 2.31 μW/cm^2 (220–280 nm), 6.94 mW/cm^2 (315–400 nm), and 129.3 mW/cm^2 (400–1050 nm), respectively. The photocatalytic reaction was triggered by turning on the light. At regular intervals, 3 mL of suspension liquid was collected by a 5 mL syringe and transferred to a centrifuge tube. After 10-min centrifugation, the clear solution was obtained. MB solution was measured by a JASCO UV–vis spectrophotometer while SCP was analyzed by a high performance liquid chromatography (HPLC, Thermo Scientific). For some tests, repeated runs were carried out and the error was found to be within 10%.

3. Results and discussion

Field emission scanning electron microscopy (SEM) was firstly used for studying the morphology of the resorcinol-formaldehyde spheres (RFSs) and carbon sphere loaded GCN samples. In Fig. 1, images of (A), (C), (E) and (G) represent 60, 200, 500 and 1000 nm RFs, respectively. The RF spheres present as uniformed spherical particles, which was used as template to produce the carbon spheres by carbonizing under inert atmosphere, shown in Fig. S1. After hydrothermal treatment with GCN, the morphologies of GCS-60, GCS-200, GCS-500 and GCS-1000 catalysts are displayed in (B), (D), (F) and (H), respectively. The carbon spheres closely attached onto the surface of layered GCN (Fig. S2) and aggregated tightly to decrease the surface energy [37]. The surface-coverage of CS decreased with increasing CS size.

The crystalline properties of various GCN and GCS photocatalysts were then investigated by XRD (Fig. 2). Two distinct peaks appeared in all the samples, which are implied as the phase (002) at 27.5° and the phase (100) at 13.1° of GCN. The two peaks are respectively contributed by the stacking fused aromatic ring and an in-planar structure of GCN. For carbon sphere loaded GCN samples,
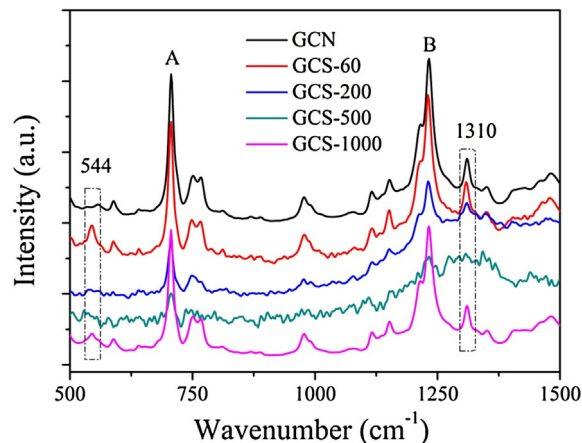
two minor peaks were appearing at 12.8° and 31.8°, respectively, These two peaks represented the newly formed "melon", the hydrolysis compound from the hydrothermal treatments of GCN at 150 °C [38]. Above results proved that the stack-layered structure of GCN could remain after the hydrothermal treatment [18]. The chemical compositions of the GCS hybrids were further investigated by FTIR spectra in Fig. S3, which shows that the GCN and GCS samples have the similar vibration bands. The absorption bands near 1570 and 1630 cm^{-1} are attributed to C=N stretching, while the three bands at 1255, 1323 and 1428 cm^{-1} are referred to aromatic C—N stretching. The peak at 809 cm^{-1} belongs to the triazin ring mode, which corresponds to condensed CN heterocycles. The band at 3150–3500 cm^{-1} corresponds to the stretching modes of groups, all belonging to the GCN material [39]. The band at 1000 and 1580 cm^{-1} are assigned to the C—O stretching and C=O stretching, respectively. [40]

Fig. 3 shows Raman spectra of the pristine GCN and the four size-controlled carbon sphere loaded GCN photocatalysts (GCS-60, GCS-200, GCS-500 and GCS-1000). A Raman shift at 544 cm^{-1} can be seen in the carbon sphere loaded GCN samples, indicating the new bond between GCN and carbon spheres. Two strong peaks at 706 (peak A) and 1230 (peak B) cm^{-1} were observed in the Raman spectra, which are assigned to the different types of ring breathing modes of s-triazine in the g-C$_3$N$_4$ crystal structure. The intensity ratios between peaks B (1230 cm^{-1}) and A (706.2 cm^{-1}) in GCN, GCS-60, GCS-200, GCS-500 and GCS-1000 are 1.05, 1.12, 1.48, 1.52 and 1.03, respectively. This value increased with CS dimensional size up to 500 nm but decreased at GCS-1000, indicating that the interaction between GCN and CS reaches the highest at CS size of 500 nm. Meanwhile, the intensities of the peaks at 544 and 1310 cm^{-1} decreased with the increasing of CS diameter until 500 nm. Those two peaks represent the bending ring and stretch ring in GCN [41], which were reduced by CS covering. The nitrogen adsorption/desorption isotherms (Fig. S4) indicate that the BET surface areas of the GCN, GCS-60, GCS-200, GCS-500 and GCS-1000 are 9.2, 8.9, 8.2, 7.9 and 5.2 m^2/g, respectively, showing decreasing surface areas with increasing CS size.

The optical properties significantly affect photosensitive capacity of the semiconductors. Fig. 4 shows UV–vis DRS of CS loaded GCN photocatalysts for evaluation of their absorption thresholds. GCN possesses a typical photosensitive semiconductor characteristic via the band gap structure [42]. GCN could absorb visible light up to 475 nm, corresponding to a bang gap energy of 2.7 eV for photo-excited electron [8]. That is attributed to the lone pair electrons of nitrogen atom in valance band jumping into the π bonding electronic conductive band [43]. All carbon sphere loaded samples (GCS-60, GCS-200, GCS-500 and GCS-1000) had similar absorption
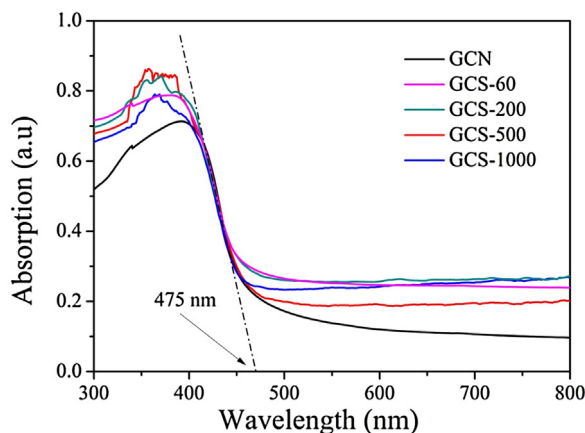
Fig. 4. UV–vis diffuse reflectance absorption of GCN, GCS-60, GCS-200, GCS-500 and GCS-1000.
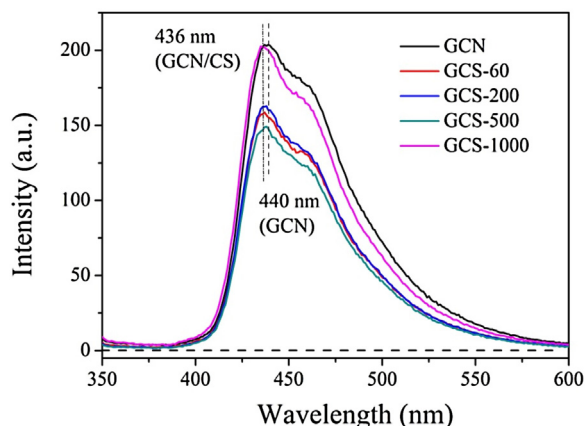

Fig. 6. Photocatalytic degradation and adsorption curves for MB over pristine GCN, GCS-60, GCS-200, GCS-500 and GCS-1000.

Fig. 5. Photoluminescence emission spectra of pristine GCN, GCS-60, GCS-200, GCS-500, GCS-1000 at 320 nm exciting radiation.

Fig. 7. SCP photodegradation by GCN, GCS-60, GCS-200, GCS-500 and GCS-1000.

as that of GCN with negligible band gap variations. However, the GCS samples presented stronger light absorption in whole UV–vis spectrum. In this study, the band structure of the GCS photocatalysts was further evaluated by the Mott–Schottky approach (Fig. S5) using an electrochemical method under 500 Mz AC voltage. The results showed that all GCS samples possess the energy potential of conduction band at around −1.0 eV (vs Hg_2Cl_2).

The photoluminescence (PL) spectra could reflect the photoelectron transit between interfaces in composite materials, which indicates the efficiency of recombination of photocarriers in photocatalysis [44]. Fig. 5 elucidates the PL-emission of pristine GCN, GCS-60, GCS-200, GCS-500 and GCS-1000 under 320 nm exciting radiations. GCN and GCS-1000 possessed the strongest emission intensities, which indicates that carbon sphere with 1000 nm slightly influences the efficiency of recombination of photoinduced charges due to too large particle size. The intensities of emission in GCS-60, GCS-200 and GCS-500 were significantly decreased after CS hybridization. In particular, GCS-500 had the lowest emission intensity among the five samples, indicating that CS could remarkably weaken the electron-hole recombination of GCN due to the size effect [34,45]. In addition, PL spectrum of GCN has a slight peak shift from 440 into 436 nm after the introduction of CS. The dislocation might represent an interaction between CS and GCN. Besides, the decrease sequence of PL emission is not following the size sequence, which may be assigned to different interaction area between CS and GCN, and thus affect the transferring efficiency of photogenerated charges.
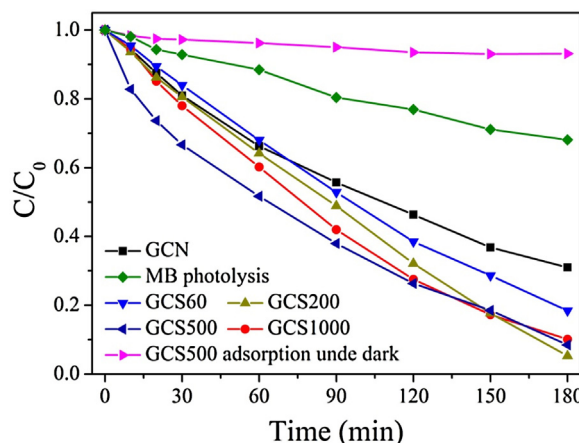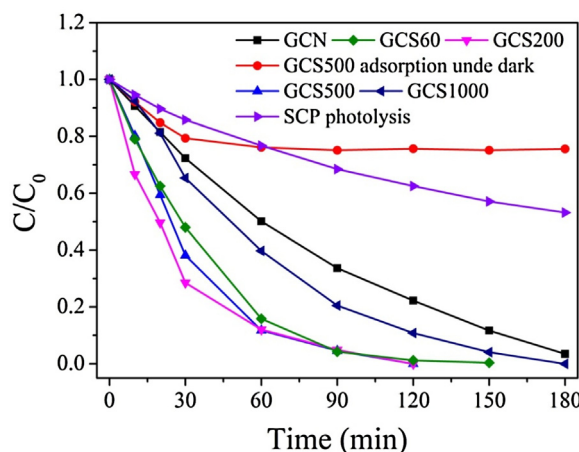
Photocatalytic performance of GCS photocatalysts were firstly evaluated through MB degradation under artificial sunlight irradiations (Fig. 6), and the degradation rates were fitted by the first order kinetics ($C_t = C_0 \cdot e^{-kt}$). All CS loaded samples have a higher activity than GCN, which could decompose about 60% MB at the end of three hours. GCS-200 could decompose 98% MB solution after three hours, presenting the best photodegradation among all the samples. GCS-60 and GCS-500 had the similar efficiency of 95%. GCS-1000 could remove about 70% MB at the same time. The reaction rate constants of GCS-60, GCS-200, GCS-500 and GCS-1000 in MB photodegradation are 0.0077, 0.0094, 0.0118 and 0.0101 min^{-1}, respectively. GCS-500 is two times higher than that of GCN ($k = 0.0066\,min^{-1}$). Furthermore, a series of GCS-500 samples at different CS loadings of 0.1, 1, 5 and 10 wt% were also prepared. It was found that 5 wt% CS on GCN sample demonstrated the best activity of MB degradation (Fig. S6).

An antibiotic of sulfachloropyridazine (SCP, 30 ppm) was also employed for evaluation of the photocatalytic degradation performances of the metal-free photocatalysts (Fig. 7). All GCS photocatalysts presented better activities than GCN and could remove about 90% SCP in 3 h. In particular, GCS-60, GCS-200 and GCS-500 could decompose all SCP within 120 min. The reaction rate constants of GCS-60, GCS-200, GCS-500 and GCS-1000 in SCP photodegradation are 0.0267, 0.0381, 0.0301 and 0.0159 min^{-1}, respectively. GCS-200 is more than three times active than that of GCN ($k = 0.0124\,min^{-1}$). GCS-500 was also tested for the catalytic stability in further four-round photocatalysis after recycling (Fig. 8).
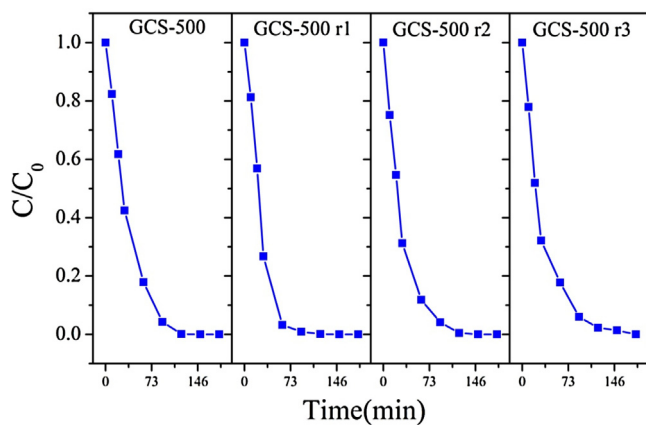
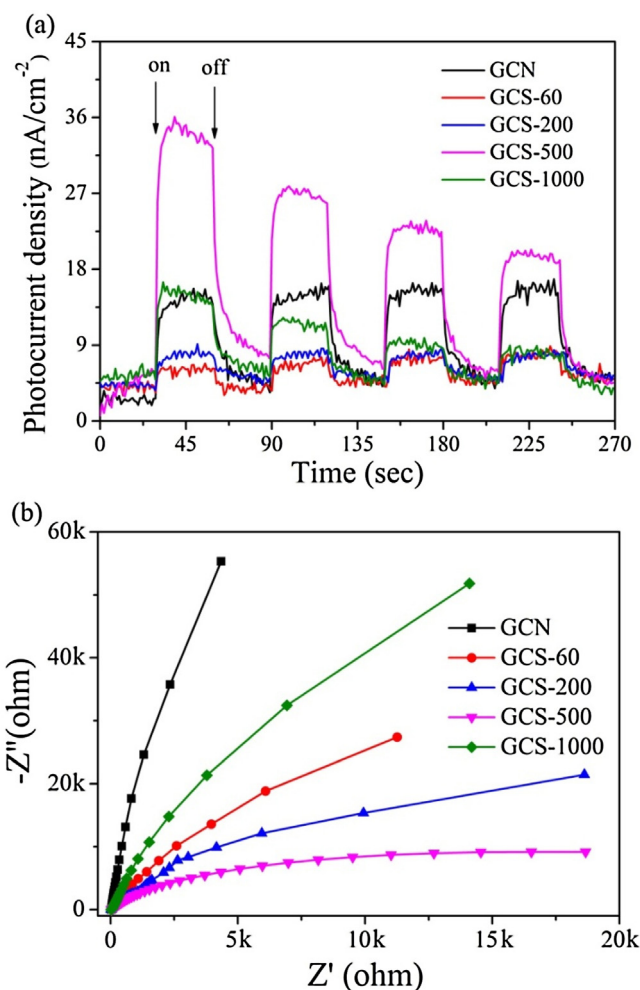Fig. 8. The stability evaluation of GCS-500 for SCP degradation.

Fig. 9. Transient photocurrent (a) and EIS curves (b) of the pristine GCN, GCS-60, GCS-200, GCS-500 and GCS-1000 in 0.1 M Na$_2$SO$_4$ solution.
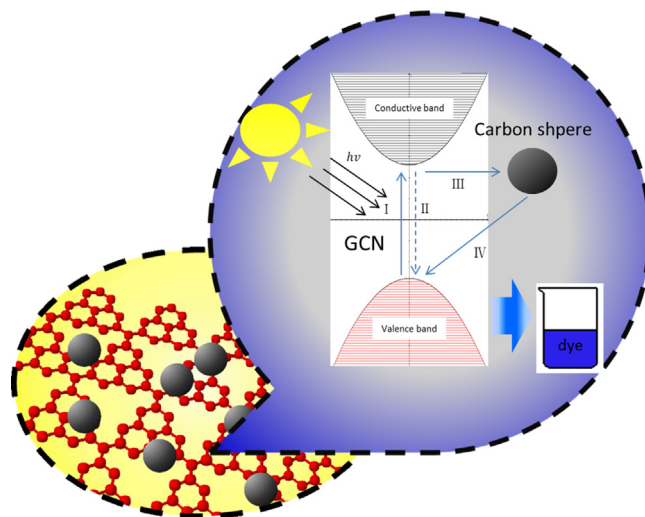

Fig. 10. Mechanism scheme of CS loaded GCN in photocatalytic degradation.

tocurrent declined gradually in 5 cycles. Photocurrents of GCS-60, GCS-200, GCS-1000 were of a similar intensity and lower than GCN, at 8 nA/cm^2. Initially, GCS-1000 had a 15 nA/cm^2 photocurrent but the photocurrent decreased to 8 nA/cm^2 at the fifth cycle. The results revealed that CS accepted the photo-electron from GCN, which can accelerate the separation of the electron/hole pairs. To further verify the relationship between photoactivity and electrochemical properties, electrochemical impedance spectroscopy (EIS) has been taken to complement the photocurrent curves to describe the transfer ability of photoinduced electrons in the samples. In Fig. 9b, the EIS spectra show that the GCS-500 possesses the smallest radius which indicates the lowest transfer barrier of electrons [46]. The sequence of radius values is consistent with the photocatalytic activity for MB and SCP. This is in accordance with the PL-spectra, which suggests that photo-electron transition leads to a weak fluorescence emission in GCS.

In photocatalysis, two radicals, superoxide radical ($^{\bullet}O_2^-$) and hydroxide radical ($^{\bullet}OH$), are believed to dominate photocatalysis in an aqueous system for organic decomposition. Two radical scavengers, *tert*-butyl alcohol and *p*-benzoquinone, were then used at a level of 1 mM to quench $^{\bullet}OH$ and $^{\bullet}O_2^-$ radicals, respectively (Fig. S7). Addition of *tert*-butyl alcohol did not show any reduction to the catalytic performance while addition of *p*-benzoquinone effectively reduced SCP degradation. Therefore, $^{\bullet}O_2^-$ generation is the key for GCS photocatalysis and $^{\bullet}OH$ will not be produced during activation of GCS by light radiation.

A mechanism based on the characterisation results and the quenching tests is thus proposed and described in Fig. 10. Carbon sphere modified GCN photocatalysts have a 2.7 eV band-gap which could absorb UV–vis light, resulting in the photogenerated electron/hole pairs (step I). After that, the photogenerated electrons are likely to move back to the valence band, recombining with the holes and emitting energy in thermal way (step II), which can be proved by a lower photoluminescence motion. At the same time, higher photocurrent generation indicates carbon sphere plays a role as electron tunnel, the photoelectron is easily transited in GCS particles. Thereby carbon sphere enables the electrons to depart from the surface of GCN (step III), thus reducing the possibility of charge carrier recombination. When the holes and electrons reach the surface of nanomaterials, the Mott–Schottky tests reveal GCS photocatalysts have about −1.0 V conductive band, which is higher enough to generate superoxide radical ($^{\bullet}O_2^-$, −0.25 V) over GCN−CS hybrid particles, the $^{\bullet}O_2^-$ could decompose MB and SCP from water, which was supported by the radical quenching experiments.

It was shown that GCS-500 maintained its catalytic activity in full decomposition of SCP in 120 min without appreciable deactivation in the four runs.

Photocurrents of the CS loaded GCN was studied by photoelectrochemical experiments (Fig. 9a). GCN-based samples produced clear transient photocurrents and with on–off irradiations, five cycles unbiased photocurrents were observed on all the samples. GCN produced a stable density of ca.15 nA/cm^2 photocurrent, while GCS-500 enlarged the photocurrent to ca.35 nA/cm^2 then the pho-

The size dependence of GCS samples can be explained by the electron drifting speed in CS. A smaller size CS (60 nm) could induce an electron transfer but meanwhile it could also make a quick combination of the electron-hole pair due to a short path. At a very large size of CS (1000 nm), an electron transfer will be much difficult. Thus, a proper size of CS (200–500 nm) can make a balance for a faster electron transfer and the lower recombination. The PL results indicate the electron transfer between GCN and CS has the best tolerant toward photoelectron at 500 nm, When the size of CS is smaller at 60 or 200 nm, the capability has been reduced. In contrast, CS at 1000 nm significantly impeded electronic pair transfer, favorable for their recombination. In photocurrent evaluation, GCS-500 sample also shows the best photo-exciting sensitivity by producing the highest current, therefore, demonstrating much high photocatalysis.

4. Conclusions

In this study, uniformed carbon spheres with varying particle sizes were prepared and used for tailoring graphitic carbon nitride to be a new metal-free photocatalyst. Carbon spheres with different sizes possess the ability to capture electrons, which could contribute to the separation of electron-hole pairs on the excited surface of GCN. The GCS-500 sample exhibited enhanced efficiency two times higher than that of the pristine GCN in MB photodegradation, and GCS-200 has a higher activity, three times higher in SCP degradation. This study suggests that GCS could be a new class of metal-free photocatalyst materials for wastewater treatment, water splitting and energy storage and the size dependence of CS particle on GCS photocatalysis.

Acknowledgement

Appendix A. Supplementary data

Supplementary data associated with this article can be found, in the online version, at http://dx.doi.org/10.1016/j.apcatb.2016.11.048.

References

[1] A.K. Geim, K.S. Novoselov, Nat. Mater. 6 (2007) 183–191.
[2] Y.W. Zhu, S. Murali, W.W. Cai, X.S. Li, J.W. Suk, J.R. Potts, R.S. Ruoff, Adv. Mater. 22 (2010) 3906–3924.
[3] K.P. Loh, Q.L. Bao, P.K. Ang, J.X. Yang, J. Mater. Chem. 20 (2010) 2277–2289.
[4] D.S. Su, S. Perathoner, G. Centi, Chem. Rev. 113 (2013) 5782–5816.
[5] L.F. Lai, J.R. Potts, D. Zhan, L. Wang, C.K. Poh, C.H. Tang, H. Gong, Z.X. Shen, L.Y. Jianyi, R.S. Ruoff, Energy Environ. Sci. 5 (2012) 7936–7942.
[6] X. Duan, H. Sun, Y. Wang, J. Kang, S. Wang, ACS Catal. 5 (2015) 553–559.
[7] X. Wang, X. Chen, A. Thomas, X. Fu, M. Antonietti, Adv. Mater. 21 (2009) 1609–1612.
[8] X. Wang, K. Maeda, A. Thomas, K. Takanabe, G. Xin, J.M. Carlsson, K. Domen, M. Antonietti, Nat. Mater. 8 (2009) 76–80.
[9] S.C. Yan, Z.S. Li, Z.G. Zou, Langmuir 25 (2009) 10397–10401.
[10] G. Liu, P. Niu, C. Sun, S.C. Smith, Z. Chen, G.Q. Lu, H.-M. Cheng, J. Am. Chem. Soc. 132 (2010) 11642–11648.
[11] Y. Zheng, Y. Jiao, J. Chen, J. Liu, J. Liang, A. Du, W. Zhang, Z. Zhu, S.C. Smith, M. Jaroniec, J. Am. Chem. Soc. 133 (2011) 20116–20119.
[12] X. Zhang, X. Xie, H. Wang, J. Zhang, B. Pan, Y. Xie, J. Am. Chem. Soc. 135 (2012) 18–21.
[13] A. Du, S. Sanvito, Z. Li, D. Wang, Y. Jiao, T. Liao, Q. Sun, Y.H. Ng, Z. Zhu, R. Amal, J. Am. Chem. Soc. 134 (2012) 4393–4397.
[14] A.Y. Liu, M.L. Cohen, Phys. Rev. B 41 (1990) 10727–10734.
[15] A. Thomas, A. Fischer, F. Goettmann, M. Antonietti, J.-O. Müller, R. Schlögl, J.M. Carlsson, J. Mater. Chem. 18 (2008) 4893–4908.
[16] L. Ge, F. Zuo, J. Liu, Q. Ma, C. Wang, D. Sun, L. Bartels, P. Feng, J. Phys. Chem. C 116 (2012) 13708–13714.
[17] J.-X. Sun, Y.-P. Yuan, L.-G. Qiu, X. Jiang, A.-J. Xie, Y.-H. Shen, J.-F. Zhu, Dalton Trans. 41 (2012) 6756–6763.
[18] X. Wang, K. Maeda, A. Thomas, K. Takanabe, G. Xin, J.M. Carlsson, K. Domen, M. Antonietti, Nat. Mater. 8 (2008) 76–80.
[19] S. Yin, J. Han, T. Zhou, R. Xu, Catal. Sci. Technol. 5 (2015) 5048–5061.
[20] Q. Xiang, J. Yu, M. Jaroniec, J. Phys. Chem. C 115 (2011) 7355–7363.
[21] Y. Xu, H. Xu, L. Wang, J. Yan, H. Li, Y. Song, L. Huang, G. Cai, Dalton Trans. 42 (2013) 7604–7613.
[22] B. Chai, X. Liao, F. Song, H. Zhou, Dalton Trans. 43 (2014) 982–989.
[23] Y.H. Ng, S. Ikeda, T. Harada, S. Higashida, T. Sakata, H. Mori, M. Matsumura, Adv. Mater. 19 (2007) 597–601.
[24] Y. Sun, C. Li, Y. Xu, H. Bai, Z. Yao, G. Shi, Chem. Commun. 46 (2010) 4740–4742.
[25] Y. Bu, Z. Chen, Electrochim. Acta 144 (2014) 42–49.
[26] C.D. Dimitrakopoulos, D.J. Mascaro, IBM J. Res. Dev. 45 (2001) 11–27.
[27] H. Sirringhaus, Adv. Mater. 17 (2005) 2411–2425.
[28] J.E. Anthony, Chem. Rev. 106 (2006) 5028–5048.
[29] L. Ming, H. Yue, L. Xu, F. Chen, J. Mater. Chem. A 2 (2014) 19145–19149.
[30] S.A. Al-Muhtaseb, J.A. Ritter, Adv. Mater. 15 (2003) 101–114.
[31] A.B. Fuertes, P. Valle-Vigon, M. Sevilla, Chem. Commun. 48 (2012) 6124–6126.
[32] R. Alcántara, P. Lavela, G.F. Ortiz, J.L. Tirado, Electrochem. Solid State Lett. 8 (2005) A222–A225.
[33] T. Horikawa, J.i. Hayashi, K. Muroyama, Carbon 42 (2004) 169–175.
[34] H. Sun, G. Zhou, Y. Wang, A. Suvorova, S. Wang, ACS Appl. Mater. Interfaces 6 (2014) 16745–16754.
[35] Y. Li, S. Wu, L. Huang, J. Wang, H. Xu, H. Li, Mater. Lett. 137 (2014) 281–284.
[37] T. Sano, S. Tsutsui, K. Koike, T. Hirakawa, Y. Teramoto, N. Negishi, K. Takeuchi, J. Mater. Chem. A 1 (2013) 6489–6496.
[38] S. Liu, H. Sun, K. O'Donnell, H.M. Ang, M.O. Tade, S. Wang, J. Colloid Interface Sci. 464 (2016) 10–17.
[39] C.-B. Cao, Q. Lv, H.-S. Zhu, Diamond Relat. Mater. 12 (2003) 1070–1074.
[40] K.S. Rao, J. Sentilnathan, H.W. Cho, J. Wu, M. Yoshimura, Adv. Funct. Mater. 25 (2015) 298–305.
[41] P.V. Zinin, L.-C. Ming, S.K. Sharma, V.N. Khabashesku, X. Liu, S. Hong, S. Endo, T. Acosta, Chem. Phys. Lett. 472 (2009) 69–73.
[42] R. Leary, A. Westwood, Carbon 49 (2011) 741–772.
[43] G. Fanchini, A. Tagliaferro, N.M.J. Conway, C. Godet, Phys. Rev. B 66 (2002) 195415.
[44] G. Liao, S. Chen, X. Quan, H. Yu, H. Zhao, J. Mater. Chem. 22 (2012) 2721–2726.
[45] F. He, G. Chen, Y. Yu, S. Hao, Y. Zhou, Y. Zheng, ACS Appl. Mater. Interfaces 6 (2014) 7171–7179.
[46] J. Ke, J. Liu, H.Q. Sun, H.Y. Zhang, X.G. Duan, P. Liang, X.Y. Li, M.O. Tade, S.M. Liu, S.B. Wang, Appl. Catal. B: Environ. 200 (2017) 47–55.

Further reading

[36] J. Liu, S.Z. Qiao, H. Liu, J. Chen, A. Orpe, D. Zhao, G.Q. Lu, Angew. Chem. Int. Ed. 50 (2011) 5947–5951.